

Impact of building envelope design parameters on diurnal building anthropogenic heat emission

Article

Published Version

Creative Commons: Attribution 4.0 (CC-BY)

Open Access

Liu, Y., Luo, Z. ORCID: <https://orcid.org/0000-0002-2082-3958> and Grimmond, S. ORCID: <https://orcid.org/0000-0002-3166-9415> (2023) Impact of building envelope design parameters on diurnal building anthropogenic heat emission. *Building and Environment*, 234. 110134. ISSN 1873-684X doi: 10.1016/j.buildenv.2023.110134 Available at <https://centaur.reading.ac.uk/111189/>

It is advisable to refer to the publisher's version if you intend to cite from the work. See [Guidance on citing](#).

To link to this article DOI: <http://dx.doi.org/10.1016/j.buildenv.2023.110134>

Publisher: Elsevier

All outputs in CentAUR are protected by Intellectual Property Rights law, including copyright law. Copyright and IPR is retained by the creators or other copyright holders. Terms and conditions for use of this material are defined in the [End User Agreement](#).

www.reading.ac.uk/centaur

CentAUR

Central Archive at the University of Reading

Reading's research outputs online



Impact of building envelope design parameters on diurnal building anthropogenic heat emission

Yiqing Liu^a, Zhiwen Luo^{b,*}, Sue Grimmond^c

^a School of the Built Environment, University of Reading, Reading, UK

^b Welsh School of Architecture, Cardiff University, Cardiff, UK

^c Department of Meteorology, University of Reading, Reading, UK

ARTICLE INFO

Keywords:

Anthropogenic heat flux
Building energy modelling
Urban climate
Parametric study
Building design

ABSTRACT

Anthropogenic heat fluxes from buildings ($Q_{F,B}$) are a major source of additional heating in cities, but vary both spatially and temporally. Knowledge of temporal variations of $Q_{F,B}$ is critical to modulate urban climate through appropriate building design. Based on a new method to determine $Q_{F,B}$ [1], this study investigates the influences of building envelope design parameters on both magnitude and diurnal pattern of $Q_{F,B}$ by season through parametric building energy modelling in Beijing. Using K-mean clustering, the distinctly representative diurnal patterns of $Q_{F,B}$ in each season are identified. With classification-based analysis, we rank building parameters to understand their roles in causing these distinct $Q_{F,B}$ patterns. We conclude that: (1) the most important building parameters influencing $Q_{F,B}$ are U-value and thermal mass. (2) U-values effectively modulate both diurnal pattern and daily magnitude in all seasons. Buildings with small U-value (e.g., U-0.2) have lower daily energy consumption, resulting in an up to 73% reduction in $Q_{F,B}$ daily mean in winter. (3) Thermal mass is more important in autumn/spring $Q_{F,B}$. It can both reduce the daily peak by up to 68% and shift the diurnal pattern dominated by mechanical cooling (peak during 15:00–17:00) into natural ventilation (peak during 01:00–06:00) with an 8–15 h lag. (4) Combined with natural ventilation, appropriate building envelope designs (e.g., small U-value with lightweight fabric) should be considered to achieve both building energy-saving and improving outdoor thermal environment. Our results could help identify useful building design strategies to mitigate urban warming/cold in the periods that are hot or cold in cities.

Nomenclature

μ_k	Centroid of each cluster
σ	standard deviation of each data in dataset
ΔBAE_{o-uo}	Difference in heat transfer by air exchange between building and atmosphere between the occupied (o) and unoccupied (uo) building ($W m^{-2}$)
C	Intra-cluster inertia of K-mean clustering algorithm
ΔH_{o-uo}	Difference in Q_H between the occupied (o) and unoccupied (uo) building ($W m^{-2}$)
$\Delta L_{t, o-uo}$	Difference in outgoing longwave radiation between the occupied (o) and unoccupied (uo) building ($W m^{-2}$)
P_k	Set of clusters
Q_{EC}	Energy consumption within building volume ($W m^{-2}$)
Q_F	Anthropogenic heat flux ($W m^{-2}$)
$Q_{F,B}$	Anthropogenic heat flux from building sector ($W m^{-2}$)
Q_{Waste}	Waste heat released to outdoor by HVAC system ($W m^{-2}$)
ΔS_{o-uo}	

(continued on next column)

(continued)

	Change in storage heat flux induced by human activities between the occupied (o) and unoccupied building (uo) ($W m^{-2}$)
T_{day}	Daily mean outdoor air temperature ($^{\circ}C$)
T_{max}	Daily peak outdoor air temperature ($^{\circ}C$)
T_{median}	Seasonal median hourly outdoor air temperature ($^{\circ}C$)
T_o	Hourly outdoor air temperature ($^{\circ}C$)
x_i	data point belonging to cluster P
\hat{x}_i	Normalised data point for clustering

1. Introduction

With decades of rapid urbanization, 69% of the global population is predicted to live in cities by 2050 [2], leading to more attention being directed to better understand the thermal characteristics of cities. Cities often experience higher nocturnal canopy layer air temperatures than surrounding rural areas (referred to as the canopy layer urban heat

* Corresponding author. Room T.14, Bute Building, King Edward VII Avenue, Cardiff, CF10 3NB, UK.

E-mail addresses: luoz18@cardiff.ac.uk (Z. Luo), c.s.grimmond@reading.ac.uk (S. Grimmond).

island, CL-UHI) [3]. This is regarded as the most apparent climate manifestation of urbanization [4]. Warmer temperatures impact building cooling energy needs, thermal comfort and human health [5–7].

The anthropogenic heat flux (Q_F) is defined as the heat converted from the consumption of biological, chemical and electrical energy and released to the atmosphere due to human activities [8]. As in dense parts of US and East Asian cities Q_F can be order of 100–500 $W m^{-2}$ (at spatial resolutions of 30 arc-seconds), it can be an important source term in the urban energy balance (Dong et al., 2017). There is consensus from urban climate modelling studies that Q_F can elevate near-surface air temperatures and strengthen the nocturnal urban heat island (e.g., Refs. [9–12]). At night (cf. daytime) the boundary layer can be relatively shallower and all energy balance fluxes, including Q_F are smaller (e.g., Refs. [10,13,14]), but its release can warm the smaller near-surface volume of air at night. For example, Fan and Sailor [4] and Bohnenstengel et al. [14] used energy consumption (Q_{EC}) as a Q_F proxy in their modelling studies and found the increases in nocturnal near-surface air temperatures of 2–3 °C (Philadelphia) and 1.5 °C (London), respectively. Hence, both the quantity of Q_F released into the atmosphere and the diurnal timing of emission are important.

Buildings ($Q_{F,B}$) account for the majority of anthropogenic heat emissions in the cities (e.g., 89–96% globally in Ref. [15]). Building occupants use energy for different activities including space heating and cooling for thermal comfort, and daily living such as lighting and other electrical appliances. The consumed energy from these activities (Q_{EC}) is eventually released from the building volume into the surroundings through convection, longwave radiation, air exchange and waste heat from HVAC system [16].

Liu et al. [1] propose a new method to estimate $Q_{F,B}$ that considers the energy fluxes that arise because of a building being ‘occupied’ (o) relative to an ‘unoccupied’ (uo) baseline when the building is assumed to be only the physical structure with both a Q_{EC} and a $Q_{F,B}$ of 0 $W m^{-2}$ [1]. The $Q_{F,B}$ emission from an occupied building (i.e., from human activities, $Q_{EC} > 0 W m^{-2}$) can arise from four heat exchange mechanisms (Fig. 1): longwave radiation ($\Delta L_{l,o-uo}$), convection (ΔH_{o-uo}), air exchange (ΔBAE_{o-uo}), and waste heat from heating/cooling system (Q_{waste}). Alternatively, $Q_{F,B}$ can be expressed in terms of the consumed energy (Q_{EC}) and changes in storage heat flux resulting from human activities (ΔS_{o-uo}) being released (absorbed) into outdoors (buildings) [1]:

$$Q_{F,B} = Q_{EC} - \Delta S_{o-uo} \quad (1)$$

Although Q_{EC} and $Q_{F,B}$ have similar magnitude for long-periods (e.g., annual, $\Delta S_{o-uo} \approx 0 W m^{-2}$), their temporal pattern can be quite different over short time scales (e.g., sub-daily, $\Delta S_{o-uo} \neq 0 W m^{-2}$). This indicates that using the diurnal profile of Q_{EC} (e.g., obtained from inventory methods) in urban climate modelling may cause bias to evaluating the $Q_{F,B}$ impact. Thus, understanding the temporal variation of $Q_{F,B}$ is crucial so that effective measures to modulate $Q_{F,B}$ and its impact on urban climate.

In the context of achieving the goal of net zero carbon, numerous

studies attempt to optimize building designs to minimize annual building energy consumption [17–19]. Theoretically, appropriate building design with minimal energy use across a year also results in the smallest magnitude of annual $Q_{F,B}$. However, these studies did not consider the variation of energy use and heat release over the time at a higher temporal resolution. The influence of different building designs on $Q_{F,B}$ at sub-daily scale has not been explained and understood yet, despite it being important in predicting variability in local-scale urban weather. Therefore, our work aims to explore and understand how typical building parameters affect the diurnal profile of $Q_{F,B}$ through parametric building energy modelling. Our results could help building and urban designers to understand how to modulate $Q_{F,B}$ in terms of magnitude and diurnal pattern through amending building parameters. Our objectives are:

- To identify the representative seasonal diurnal patterns of $Q_{F,B}$ and to provide a method for doing this.
- To understand which building parameters are important in controlling the seasonal $Q_{F,B}$ pattern
- To provide insight on how the important building parameters cause different $Q_{F,B}$ profiles.

2. Methods

This study is based on the Liu et al. [1] method to estimate $Q_{F,B}$ that considers the difference in energy balance fluxes between occupied (o) and unoccupied (uo) building (Eq. (1), Fig. 1). Building energy simulations are undertaken for one-year for both the o and uo states (i.e. with the same building fabric) allowing 365 $Q_{F,B}$ diurnal profiles to be calculated for 600 building cases (i.e. unique combination of building parameter value in Table 1). Clustering is used to identify the main representative diurnal patterns of $Q_{F,B}$ in each season and help understand the relation between pattern distribution and building parameters.

2.1. Parametric building energy simulation

The multi-parametric building energy simulations use the Liu et al. [1] *ov3* simplified residential building case, assuming continuous occupation (i.e. 24-h per day) with thermal comfort achieved by

Table 1
Parameter types and values used in simulations (600 cases).

Parameters	Units	Discrete values used
Windows orientation	°	0, 90, 180, 270
Windows wall ratio	%	10, 20, 30, 40, 50
Thermal mass	$kJ m^{-2} K^{-1}$	Heavyweight (404.5), mediumweight (148.5), lightweight (96.0)
Insulation position	–	External, internal
Thermal transmittance (U-value)	$W m^{-2} K^{-1}$	0.2, 0.3, 0.5, 1.0, 2.1

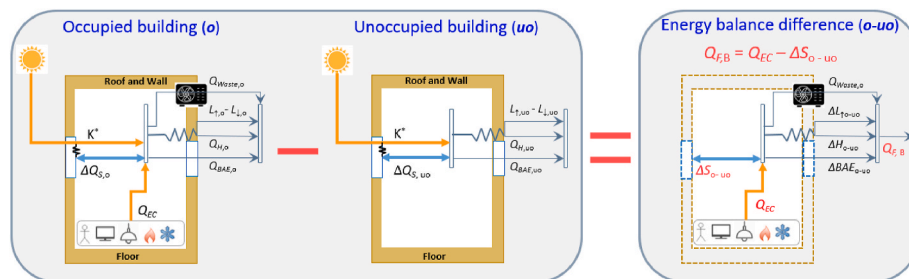


Fig. 1. Schematic of principles used to derive anthropogenic heat emission from buildings ($Q_{F,B}$) by considering the differences in heat fluxes between an ‘occupied’ (o) and ‘unoccupied’ building (uo). Adapted from Ref. [1].

changeover mixed-mode ventilation and HVAC. The building geometry uses the ASHRAE standard 140 Case 900 test model with a south-facing window and single-sided ventilation (ASHRAE, 2017). The window area is 10% openable if the indoor air temperature is warmer than both the outdoor air temperature and the ventilation setpoint (23 °C). The idealised HVAC system has fixed heating (18 °C) and cooling (26 °C) setpoints. With a centralised heating system (as Beijing has [20]), for simplicity we assume all energy associated with the heating system is released indoors, and waste heat due to boiler efficiency and pipe heat loss are not considered. The waste heat from cooling system (e.g., including cooling load and cooling energy consumption) is assumed to be emitted to the outdoors immediately.

The unoccupied building (*uo*) baseline is assumed to be ideally sealed but with the same building envelope parameter values as the occupied building (*o*). The explored building parameters (Table 1) are selected to represent both those used in early building design decisions, and whose impact on building performance have been widely explored, such as energy usage index [17–19] and overheating risk [21–23].

Thermal mass, thermal resistance, and position of insulation layer are the three most crucial factors for the dynamic thermal behaviour of multi-layer building fabrics [24,25]. Here three thermal mass levels are considered whose surface areal heat capacity (e.g., wall) ranges from 96.0 to 404.5 kJ m⁻² K⁻¹. Different thermal mass levels are achieved by modulating the thickness of massive material (detailed information for building components characteristics given in supplementary material Table S.1-3). Note, the specified thermal mass (Table 1) is the average area heat capacity for all layers of construction material, independent of insulation position. The impact of thermal mass and insulation position (i.e., insulation layer external or internal to massive material for wall and roof) is analysed separately (Table 1).

As the U-value and solar heat gain coefficient (SHGC, i.e., fraction of solar radiation transmitted through windows) of thermal properties are treated together (i.e. opaque components and windows) in the local building code in China [26–28], we combine them to create five thermal properties levels that satisfy the requirement of improving energy efficiency. The U-value variations are achieved by modifying the thickness of insulation layer in external wall and roof (Table S.1, S.2). The two extreme cases (U-0.2 and U-2.1) have the best and poorest insulation (no insulation for heavyweight construction) respectively. Values assigned (Table 1) span the physically reasonable to ensure appropriate variation in simulation cases.

With the aim of having a theoretical understanding of how the fundamental parameters affect the diurnal variation of $Q_{F,B}$, each value assigned to a parameter is discrete and has equal probability. Hence, 600 cases are simulated for one-year with Beijing climate forcing [29] by

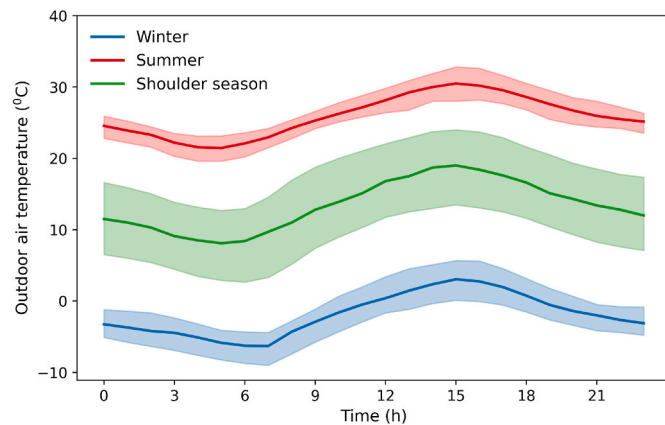


Fig. 2. Seasonal diurnal median (line, T_{median}) and interquartile range (IQR, shading) outdoor air temperature in Beijing [29]. Shoulder season refers to spring and autumn. Seasons are defined by months (e.g., Summer: JJA (June, July, August), Winter: DJF).

using the jEPlus [30] parametric tool to execute EnergyPlus [31]. Beijing is chosen for its climate with distinct seasons (Fig. 2), with both cold winters (T_{median} diurnal range: -6.3 to 3.1 °C) requiring heating and hot summers (T_{median} diurnal range: 21.5 – 30.5 °C) requiring cooling. The milder shoulder seasons (spring and autumn) has larger day-to-day variation (IQR shading, Fig. 2). This study can be extended easily to other climates.

2.2. K-mean clustering

The diurnal temporal pattern of $Q_{F,B}$ indicates when, and how, it may impact the urban environment. The patterns vary with building parameters and weather conditions, and has a direct influence on building energy use and storage heat flux. Pattern identification commonly involves an algorithm that clusters from a data into several groups with high similarity [32]. Here the simulation results dataset (section 2.1) is used to identify the $Q_{F,B}$ representative diurnal patterns.

Although no agreement exists in the literature to the ‘best’ clustering algorithm, studies indicate K-mean clustering provides both good performance for pattern identification and a stable cluster result [33,34]. Furthermore, it is one of the most widely applied algorithms for identifying electricity load patterns or building energy use profile [35–37]. Hence, we select it for this study.

Given a dataset with a large number of diurnal profiles, K-mean clustering algorithm classifies all the profiles into pre-defined number (K) of clusters. The classified profiles are ‘similar’ within a cluster but ‘dissimilar’ to other clusters.

An iterative process is used with the objective to minimize the intra-cluster inertia [36]:

$$C(P, \mu) = \sum_{i=1}^n \sum_{x_i \in P_k} \|x_i - \mu_k\|^2 \quad (2)$$

where $P_k = (P_1, P_2, \dots, P_k)$ is the set of clusters, $\mu = (\mu_1, \mu_2, \dots, \mu_k)$ is the centroid of each cluster, x_i is the data point belonging to P_k . The main steps are to (e.g., [34]): (a) initialize K number of centroids (μ) randomly, (b) assign each point from dataset to nearest centroid by minimizing $C(P, \mu)$, (c) update the new centroids to the mean in each cluster, and (d) repeat (b) and (c) until convergence occurs.

Since the impacts from the building parameters could differ between seasons, the $Q_{F,B}$ diurnal profiles (section 2.1) are sub-divided into three periods groups: winter (December, January and February, DJF), summer (JJA) and shoulder season (MAM-SON). Every 10th $Q_{F,B}$ diurnal profiles is selected for all building cases, which reduces the day-to-day variability but retains the intra-season synoptic variability. This results in 5400 profiles for both winter and summer, and 10800 profiles in the shoulder season, to be analysed (i.e., 3 groups) with K-mean clustering.

Prior to analysis, the diurnal profile are normalised to capture pattern shapes and avoid negative influence of absolute magnitude [38] (using the Z-score method [37]):

$$x'_i = (x_i - \bar{x}) / \sigma \quad (3)$$

where x_i is the hourly $Q_{F,B}$, $i \in [0, 23]$, \bar{x} is mean and σ standard deviation of each $Q_{F,B}$ diurnal profile.

As the number of clusters needs to be pre-defined, but the truth is no agreed method to determine the optimal number. Some metrics are used (e.g., silhouette score [39], and Calinski-Harabasz (CH) Score [40]) balance the intra-cluster similarity and inter-cluster differences. However, we want to find the most representative patterns and understand the impact of building parameters on pattern variance. The clustering derived patterns are expected to be sufficiently distinct and the separation between clusters could be more important. To select the suitable value for K we use the ‘clustergram’ algorithm [41], which plots a wide range of K values alongside the weighted mean of the first component of a principal component analysis (PCA) in each cluster which indicates the

variance of cluster performance. This method demonstrates how the dataset could be split between clusters by changing K (Fig. 3). Analysis of winter data indicates the optimal K is 3, gives a clear separation between clusters (Fig. 3). When K increases from 4 to 6, some points are rather close or overlap (i.e., clusters have similar diurnal patterns), making analysing the effect of building parameters on their difference more difficult. The same analysis is repeated for other seasons. The appropriate K are selected in Table 2. The K-mean clustering and relevant data processing step are summarised in Fig. 4.

2.3. Decision tree classification

The classification and regression tree (CART) algorithm is used [42] to understand the relative importance of building parameters on diurnal patterns of $Q_{F,B}$. Binary splitting of input features space (i.e. building parameters values, Table 1) the algorithm disaggregates the target feature (i.e. diurnal patterns of $Q_{F,B}$ from clustering) into smaller subsets with higher similarity. The partitioning roles are constructed by minimizing the impurity of subsets (i.e. Gini index [43]) after the binary split at each node. This helps to build understanding of how selected building parameters values affect diurnal patterns and output a rank of relative importance.

3. Results and discussion

3.1. Winter

From clustergram analysis in winter (Fig. 3) an optimal value for K of 3 is chosen. The three sets of data have distinct diurnal variations (Fig. 5a–c). The cluster with the most profiles (60%) is *winter0*. For this cluster the peak of the normalised $Q_{F,B}$ is typically in the early morning (07:00), after which it decreases to a valley in the afternoon (16:00). For *winter1* the peak is about 2 h later than *winter0*, but it stays positive (i.e., hourly $Q_{F,B} >$ daily mean) until 16:00 (i.e., around sunset). Whilst *winter2* has bimodal daytime peaks (07:00 and 15:00), the nocturnal and mid-day values are small (Fig. 5c). The human behaviours for modulating indoor thermal comfort have negligible difference among three clusters as mechanical heating systems are warming the building most of time (orange, Fig. 5d–f).

To identify the relative importance of the building parameters on the cluster $Q_{F,B}$ diurnal patterns the CART [42] algorithm is used (section 2.3). The U-value and thermal mass are found to be the most critical parameters (cf. others, Fig. 6) in determining the $Q_{F,B}$ diurnal patterns in winter (red, Fig. 6), accounting for 68.4% and 21.4% of feature importance respectively.

Small U-values (0.2, 0.3) cause *winter0* to be the dominant $Q_{F,B}$ pattern (Fig. 7a). With better insulation, heat loss through conduction is reduced and in return less heating is required (median peak Q_{EC} *winter0* = 41 W m⁻²; cf. *winter1* = 87 W m⁻²; *winter2* = 77 W m⁻²). Smaller Q_{EC}

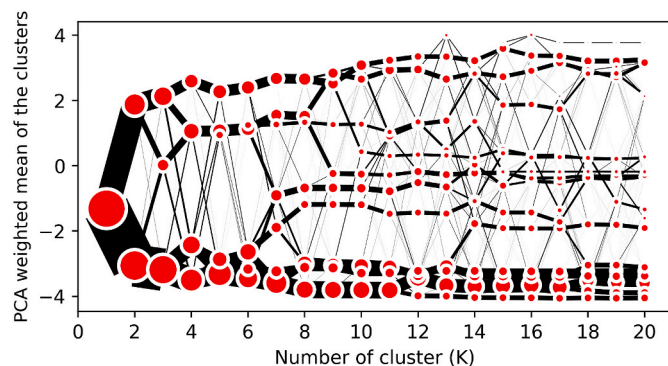


Fig. 3. Clustergram of the potential K for initial partitioning of $Q_{F,B}$ diurnal patterns in winter.

Table 2
Clustergram analysis to determine the number of clusters K.

Period	Variable	Objectives	Building cases	# days	Suitable K
Winter	$Q_{F,B}$	Normalised diurnal profile	600	9	3
Summer	$Q_{F,B}$	Normalised diurnal profile	600	9	4
Shoulder season	$Q_{F,B}$	Normalised diurnal profile	600	18	4

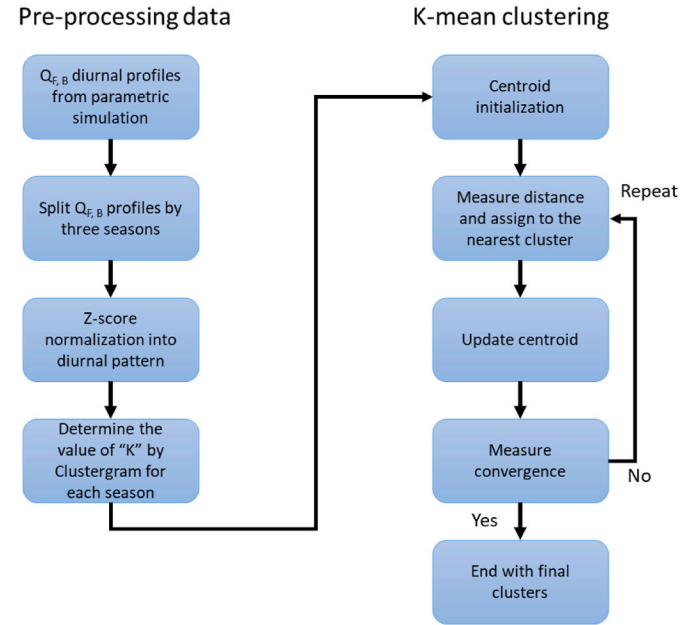


Fig. 4. Flowchart of data pre-processing and K-mean clustering steps undertaken.

throughout the day results in a small change in heat storage flux (ΔS_{0-10}) (*winter0* median peak = 4.4 W m⁻²; Fig. 7e). Consequently, $Q_{F,B}$ (= $Q_{EC} - \Delta S_{0-10}$) keeps the same temporal phase as Q_{EC} but with less fluctuation. Small U-values are linked to small daily mean $Q_{F,B}$ (Fig. 7b), suggesting buildings with more insulation (e.g., new construction), not only consume less Q_{EC} but also release less $Q_{F,B}$. The winter $Q_{F,B}$ diurnal cycle is out-of-phase with typical outdoor air temperature (Fig. 7c).

With high U values (2.1), $Q_{F,B}$ and Q_{EC} patterns differ and thermal mass impacts the diurnal shape. *Winter2* is linked to heavy thermal mass (Table 1), while medium and light weight are more likely *winter1* (Fig. 7a). No (or little) insulation leads to considerably higher heating energy demand resulting in larger variability of ΔS_{0-10} . The difference between *winter2* and *winter1* patterns is explained by the influence of thermal mass on Q_{EC} and ΔS_{0-10} .

With warmer daytime outdoor air temperatures and solar radiation, heavyweight fabric absorbs more heat (cf. lightweight), consequently more heating energy is required to maintain the indoor air temperature. Conversely, the release of stored heat can reduce heating demand at night when outdoor air and external surface temperatures decrease. This is consistent with *winter2* (heavyweight) Q_{EC} being greater than *winter1* (light/medium weight) between 12:00 and 19:00 (Fig. 7d). *Winter2* allows a continuous increase of ΔS_{0-10} with increasing Q_{EC} at night, while ΔS_{0-10} in *winter1* stops increasing at 03:00 then decreases to become negative 3 h earlier than *winter2* due to limited heat capacity. The earlier release of stored heat causes a higher $Q_{F,B}$ from 09:00 in *winter1*. While *winter2* starts to release stored heat after 13:00, causing the second peak $Q_{F,B}$ in the afternoon.

Winter1 and *winter2* could represent buildings constructed many

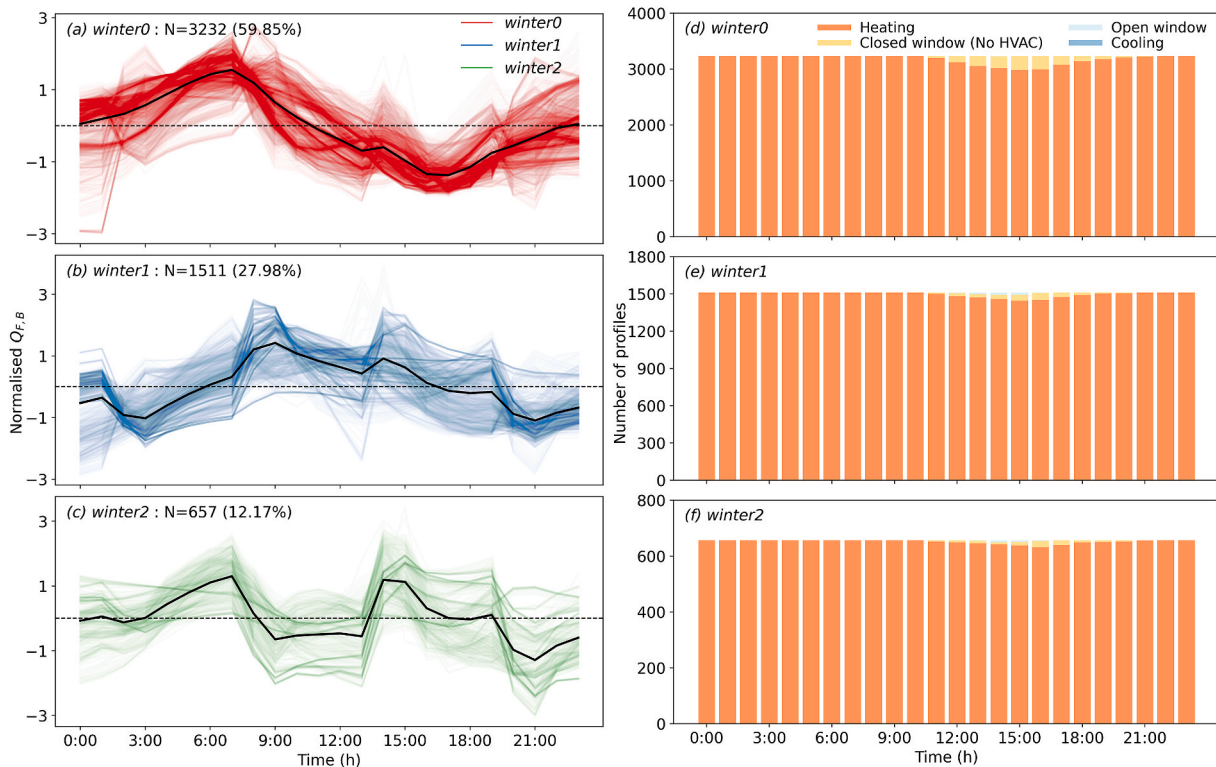


Fig. 5. After clustering of winter profiles for $K = 3$, the (a–c) diurnal patterns, and (e–f) building operations for the three clusters (a,d) *winter0*, (b,e) *winter1*, (c,f) *winter2* with the number (N) of profiles within the cluster, its relative percentage, and mean (black line).

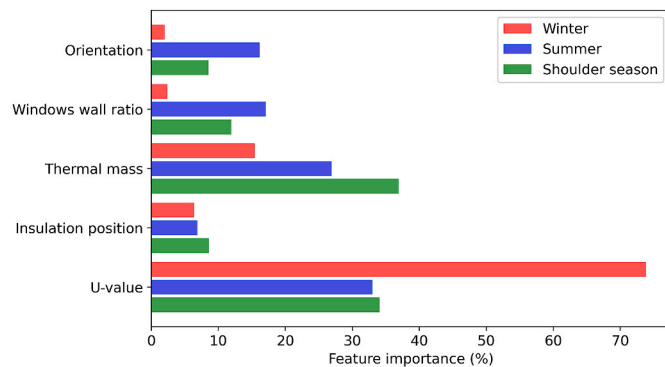


Fig. 6. Relative importance of building parameters on $Q_{F,B}$ diurnal patterns for different seasons clusters.

decades ago without energy-saving retrofitting. Lacking sufficient insulation, more heating energy is consumed resulting in a large daily mean $Q_{F,B}$ (101.8 and 100.7 W m^{-2} for lightweight and mediumweight respectively in Fig. 7b). Use of heavyweight fabric could delay part of $Q_{F,B}$ release in the afternoon and have a slight reduction in daily mean $Q_{F,B}$ (93.7 W m^{-2} in Fig. 7b). For the remaining building groups (i.e. U-1.0, U-0.5), three clusters coexist because different weather conditions and other parameters also impact diurnal pattern to some extent. The combination of smaller U-value and heavier fabric leads to a larger fraction of cluster of *winter0*, otherwise, *winter1* dominates the pattern. The coexistence of multiple patterns indicates the diurnal shapes of this combination of building parameters are less consistent and/or more easily impacted by other factors (e.g., insulation position, windows wall ratio orientation and weather).

Overall for winter, the role of insulation on both diurnal pattern and magnitude of $Q_{F,B}$ is critical. Improving insulation is a promising measure to effectively modulate the diurnal pattern and reduce the daily

mean magnitude of $Q_{F,B}$. With U-values >0.5 , the change of heat storage flux becomes more important. Thermal mass distinguishes the diurnal patterns but has limited impact on daily mean magnitude.

3.2. Summer

In summer, K is set to four, creating four clusters of diurnal patterns (Fig. 8). They can be categorised into two groups based on human behaviour for thermal comfort. *Summer0*, *summer1* and *summer2* are mainly dominated by mechanical cooling, therefore they have similar diurnal cycles but different time phases. Their peak values occur between 15:00–18:00 linked to timing of the largest cooling demand and waste heat release. These days have peak outdoor air temperature (T_{\max}) of 29.8 – $34.4 \text{ }^\circ\text{C}$.

Whereas *summer3* occurs only on 5th June when the outdoor temperatures are mild ($T_{\max} = 24.4 \text{ }^\circ\text{C}$) and suitable for natural ventilation (Fig. 8h). At night $Q_{F,B}$ peaks due to high indoor and outdoor heat exchange by natural ventilation, whereas, the minima occur mid-afternoon when the warm outdoor temperature limits natural ventilation but some cases yet needs mechanical cooling. The *summer3* have small U-values or heavyweight fabric (Fig. 9a), suggesting buildings with these attributes can be cooled by natural ventilation when the outdoor air temperature is not very high. Whereas buildings with larger U-values (also larger solar heat gain coefficient (SHGC, i.e., fraction of solar radiation transmitted through windows)) and less massive fabric, receive more solar gain through windows but lack sufficient heat capacity to dampen indoor air temperature. Mechanical cooling is used despite mild weather, leading to other summer patterns.

To maintain indoor air temperature throughout the day in *summer0-2*, space cooling dominates, leading to similar $Q_{F,B}$ patterns among them, which follow the corresponding Q_{EC} shapes (varying with cooling energy) (Fig. 9c and d). *Summer1* peaks earliest (15:00), whilst *summer0(2)* is delayed by 23 hours. Change in cluster proportions reveals how U-value and thermal mass alter the time phase (Fig. 9a).

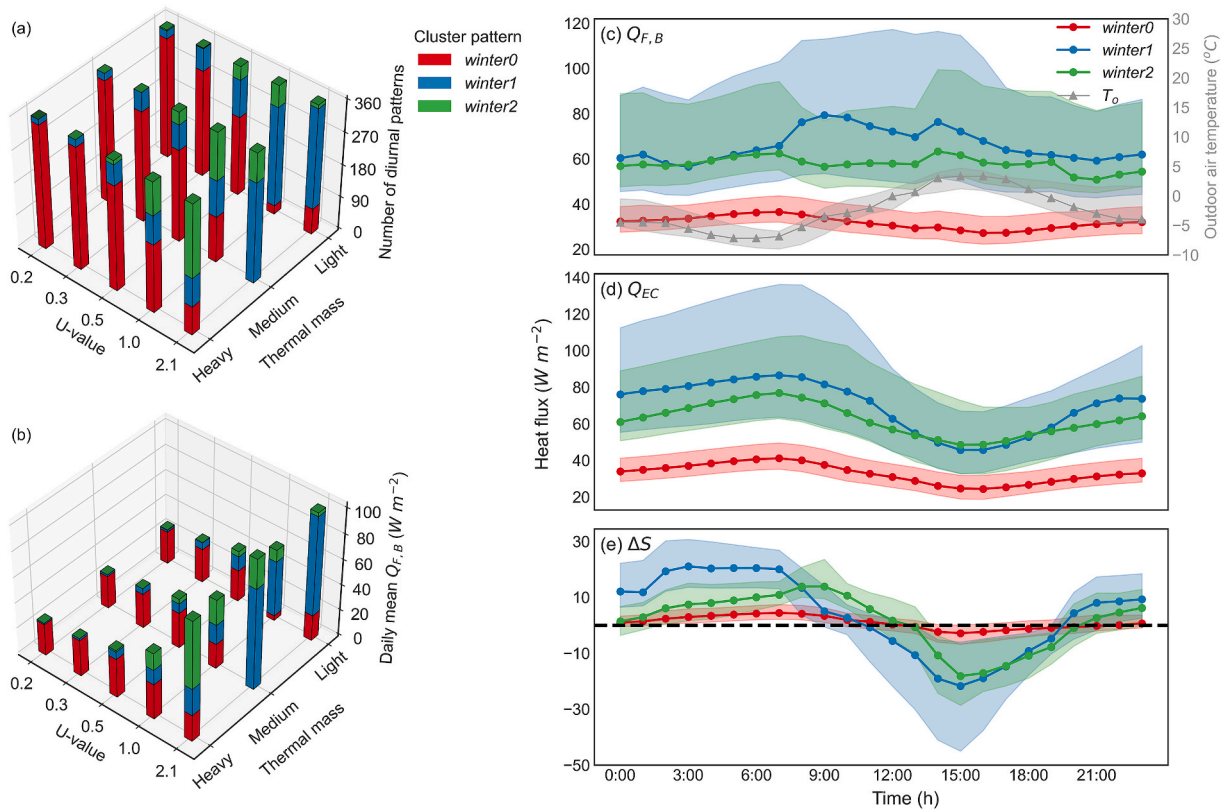


Fig. 7. Three winter clusters (colour) relation with (a, b) building parameters (U-value and thermal mass) and (a) number of profiles ($N = 360$) and (b) daily mean $Q_{F,B}$; and (c–e) median (line) and interquartile range (IQR, shading) diurnal pattern of (c) $Q_{F,B}$, (d) building energy consumption (Q_{EC}) and (e) change in storage heat flux from human behaviour (ΔS_{0-10}). (For interpretation of the references to colour in this figure legend, the reader is referred to the Web version of this article.)

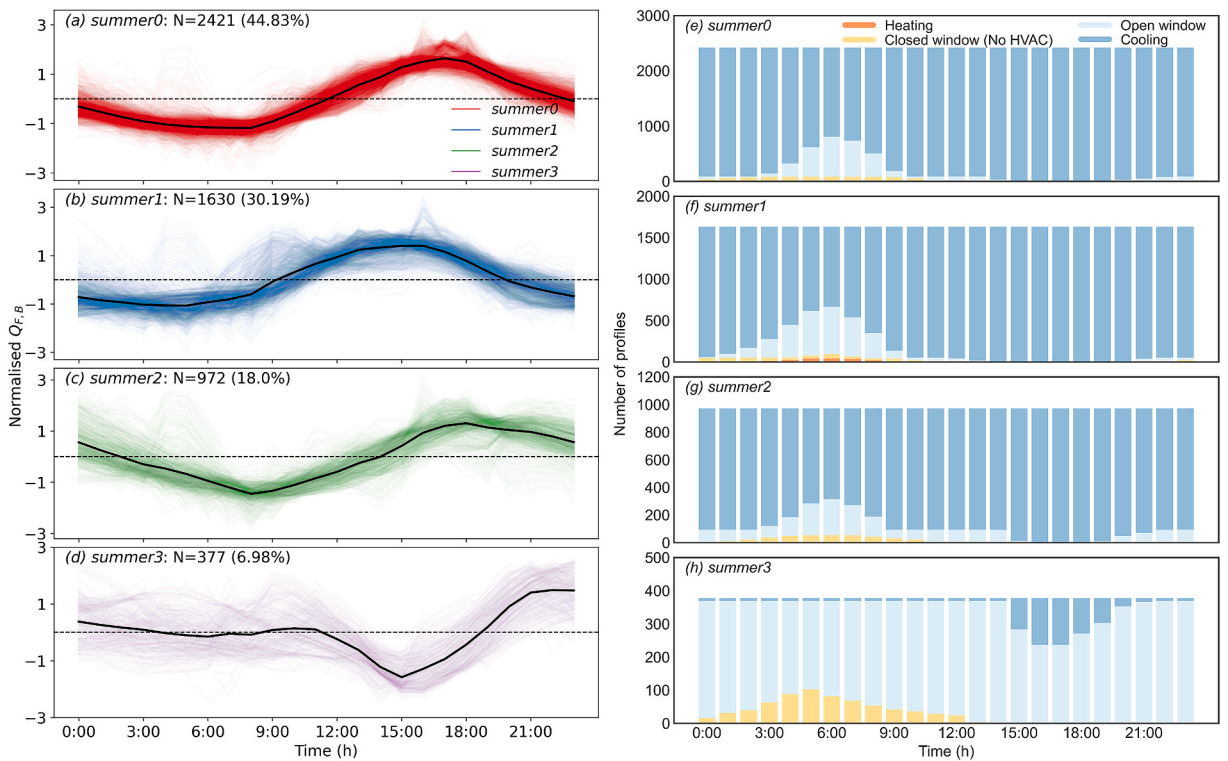


Fig. 8. As Fig. 5, but for summer with $K = 4$.

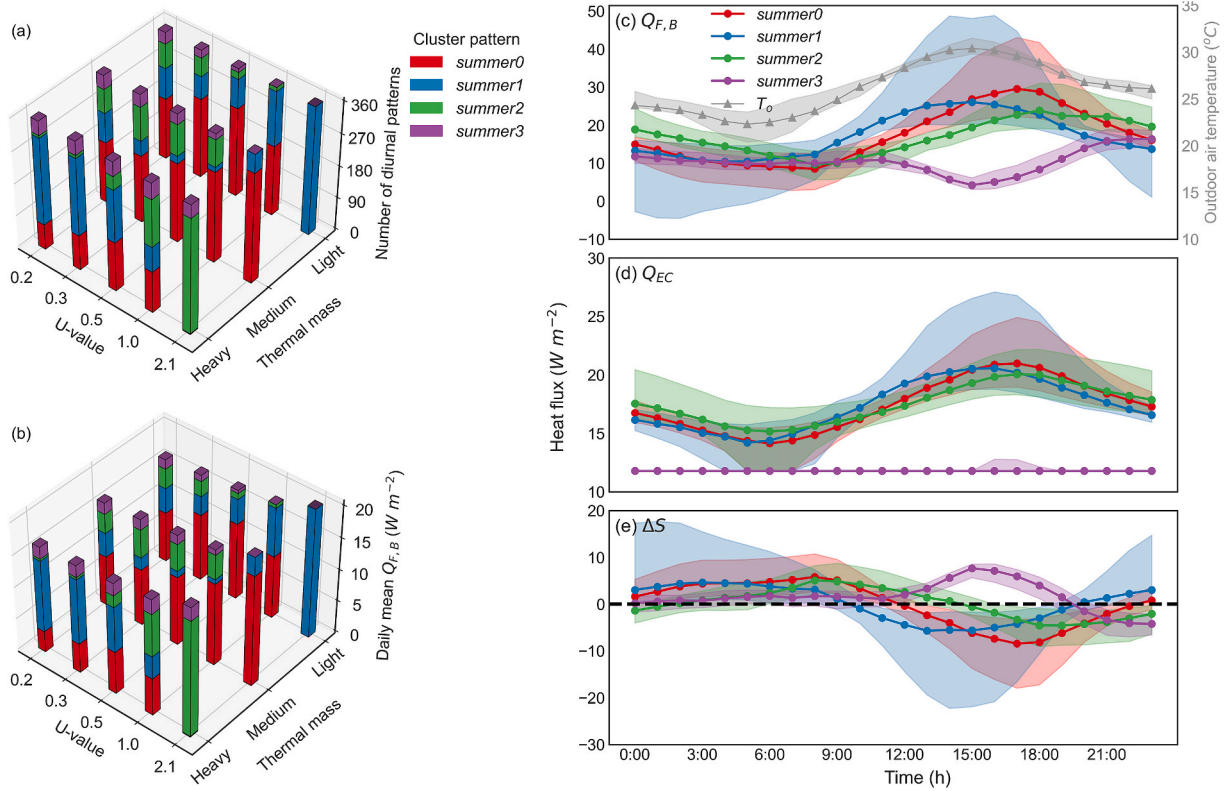


Fig. 9. As Fig. 7, but for summer.

Unlike in *winter*, the effect of thermal mass can be the opposite for the two extreme U-values. For U-2.1, the dominant pattern changes from *summer1* to *summer2* with increasing thermal mass, indicating the peak $Q_{F,B}$ can be lagged if there is a higher heat capacity. It is consistent with the general expectation that larger heat capacity fabric stores more heat during the daytime, therefore delays the peak of cooling demand and $Q_{F,B}$. Whereas, *summer1* cases increase is linked to heavier fabric when the U-value is small (0.3 and 0.2) (Fig. 9a), suggesting an earlier peak will occur with increasing thermal mass. Heavyweight fabric stores more heat than lightweight fabric during the daytime. At night, such stored heat is trapped by high-level insulation, and cannot be dissipated by convection and longwave radiation until it is at the external surface. On the next day, heavyweight buildings have an earlier $Q_{F,B}$ peak. This agrees with others' finding that increasing thermal mass may cause larger cooling demand at night in the dwelling when the insulation level is high [44].

Similarly, the compensating effect between the U-value and thermal mass leads to contradicting roles in modulating $Q_{F,B}$ pattern phases for lightweight and heavyweight buildings. Hence, the impact of thermal mass and U-value cannot be determined independently, which is consistent with the conclusion that additional insulation may reduce or exacerbate overheating risk in summer [23]. In addition, varying U-value causes negligible change to the daily mean $Q_{F,B}$ (Fig. 9b) due to compensating effects of improving opaque insulation and windows properties. Theoretically, smaller SHGC from windows (e.g., apply double or triple glazing windows) would effectively reduce building heat gain and cooling demand [18,45]. But improved insulation traps nocturnal heat when outdoor environment is sufficiently cool, subsequently more stored heat may increase cooling energy use on the next day.

In summary, despite limited change in daily mean magnitude, both U-value and thermal mass can modulate the timing of $Q_{F,B}$ diurnal pattern in response to when buildings are occupied (i.e., $o - uo$), which may lead to different impacts on urban climate. For example, new

construction with excellent insulation and heavyweight fabric could advance the $Q_{F,B}$ peak during the daytime, resulting in less nocturnal heat release when the boundary layer is shallow. Whilst lightweight fabric may be more suitable for building with less insulation in term of reducing nocturnal heat release and mitigate urban heat island. It is critical that both U-value and thermal mass are considered by building designers as they jointly determine the timing phase.

3.3. Shoulder season

The four clusters (Fig. 10) in the shoulder season are a combination of winter and summer patterns. *Shoulder0* and *shoulder3* (Fig. 10a and d) are similar to *winter0* and *winter1* (Fig. 5 a and b) with heating dominating the building operation. Whilst, *shoulder1* and *shoulder2* (Fig. 10b and c) have patterns similar to *summer0* and *summer3* (Fig. 8a and d) with natural ventilation and mechanical cooling dominating. Such similarities indicate the $Q_{F,B}$ patterns in shoulder season are linked with the weather transitions.

Unlike in winter or summer, with only one dominant building operation mode per cluster, all shoulder season clusters have multiple operations modes during the course of the day, because of the wide weather range (e.g., daily mean air temperature (T_{day}) ranges from 1.7 °C to 21.5 °C). This makes understanding the influence of building parameters on $Q_{F,B}$ patterns more challenging. To reduce the weather variability, we separate the profiles into cool (MON [March, October and November, T_{day} : 1.7 °C → 12.2 °C]) and warm (AMS [T_{day} : 10.1 °C → 21.5 °C]) months.

The cool months dominant pattern and impacts of envelope thermal properties are highly consistent with winter scenario (Fig. 11a). The *shoulder0-a* (53%) and *shoulder3-a* (25%) are nearly identical to *winter0* and *winter1* (Fig. 5a and b) because of a Q_{EC} diurnal cycle linked to space heating. Higher heating demand in *shoulder3-a* contributes to larger change in heat storage flux (ΔS_{o-uo}) and different $Q_{F,B}$ patterns to Q_{EC} . U-value is also the most important factor determining the pattern and daily

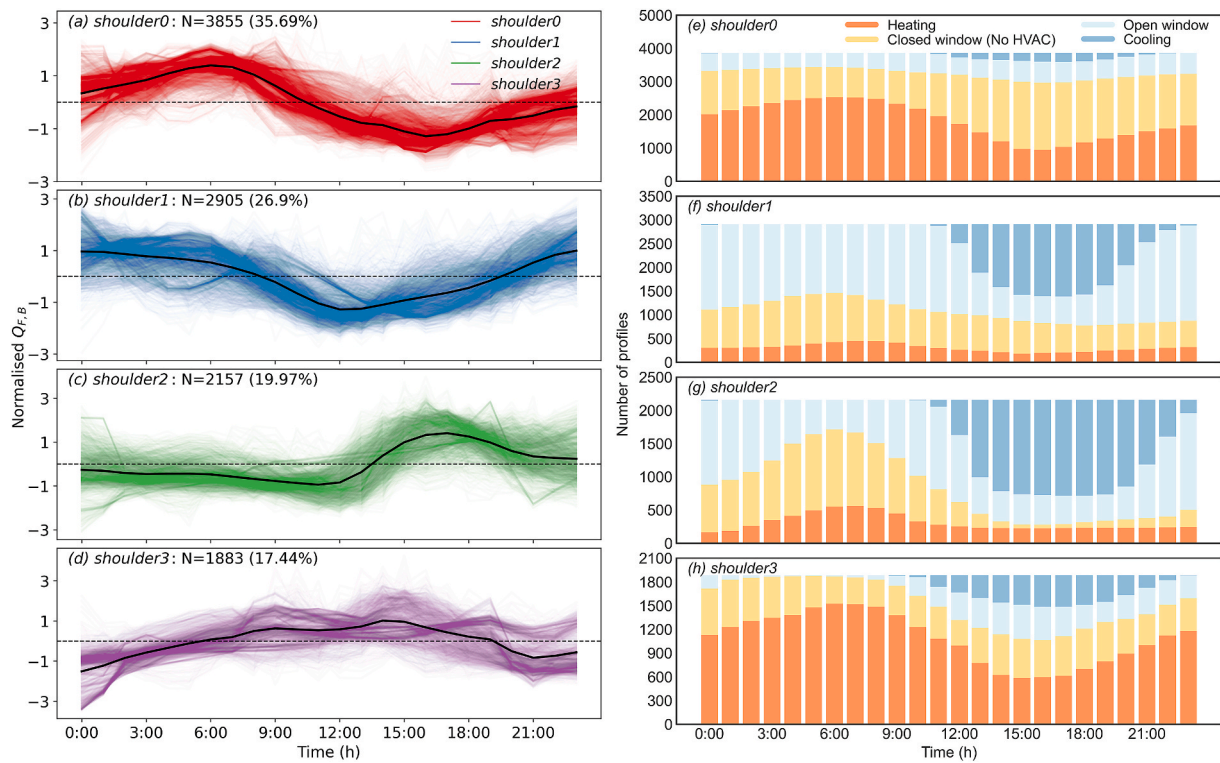


Fig. 10. As Fig. 5, but for the shoulder season with $K = 4$.

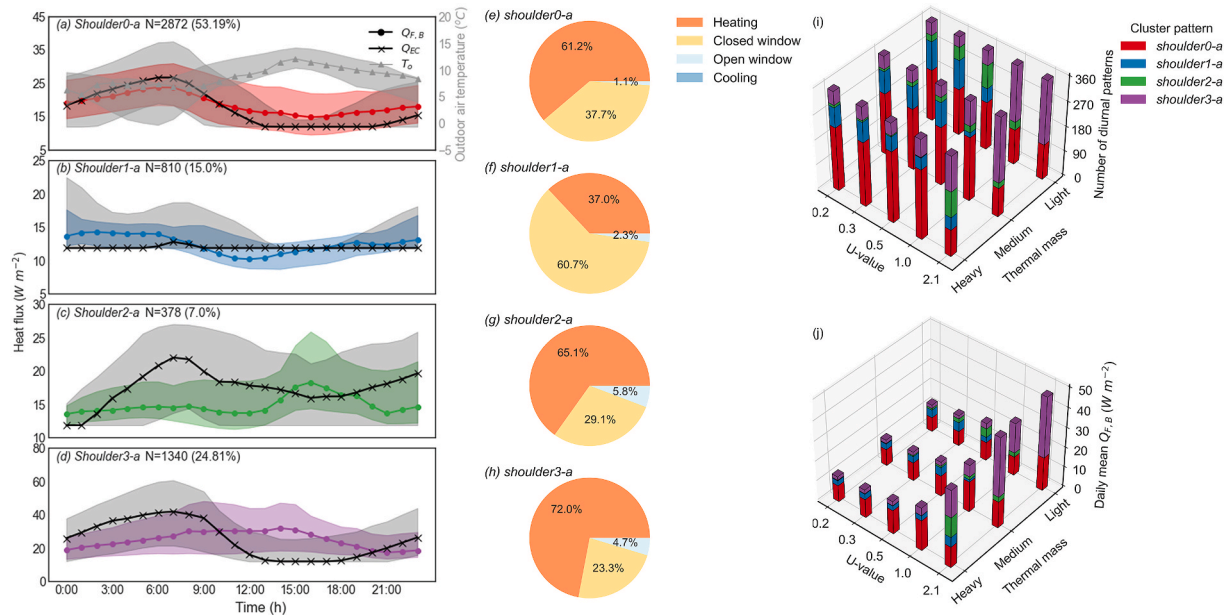


Fig. 11. Shoulder season in March, October and November (MON) (a–d) median (line) and interquartile range (IQR, shading) diurnal pattern of $Q_{F,B}$ and Q_{EC} and (e–h) corresponding building operation mode proportions for four clusters (a, e) *shoulder0-a*, (b, f) *shoulder1-a*, (c, g) *shoulder2-a* and (d, h) *shoulder3-a*. Four cluster (i) pattern and (j) magnitude relation with building parameters (U-value and thermal mass) as in Fig. 7(a and b).

mean distribution (Fig. 11i and j).

Poor insulation (U-2.1) is important in *shoulder3-a* (more heat is released). With improved insulation, less heating is required and *shoulder0-a* becomes the main pattern. *Shoulder1-a* can be regarded as an extension of *shoulder3-a* to *shoulder0-a* when less heating is required. Thus, its frequency increases with decreasing U-value, implying the buildings with more insulation release less $Q_{F,B}$. More use of insulation could effectively reduce both energy use and corresponding heat release

in this season.

In the warm months (AMS), natural ventilation become more important and both U-value and thermal mass play crucial roles in distinguishing human behaviour and corresponding $Q_{F,B}$ pattern. *Shoulder3-b* (Fig. 12d) has dual Q_{EC} peaks as building is heated at night but mechanically cooled in the afternoon. This mainly occurs in building cases with a combination of U-2.1 and lightweight (Fig. 12i), due to lacking thermal resistance and thermal inertia to dampen the indoor

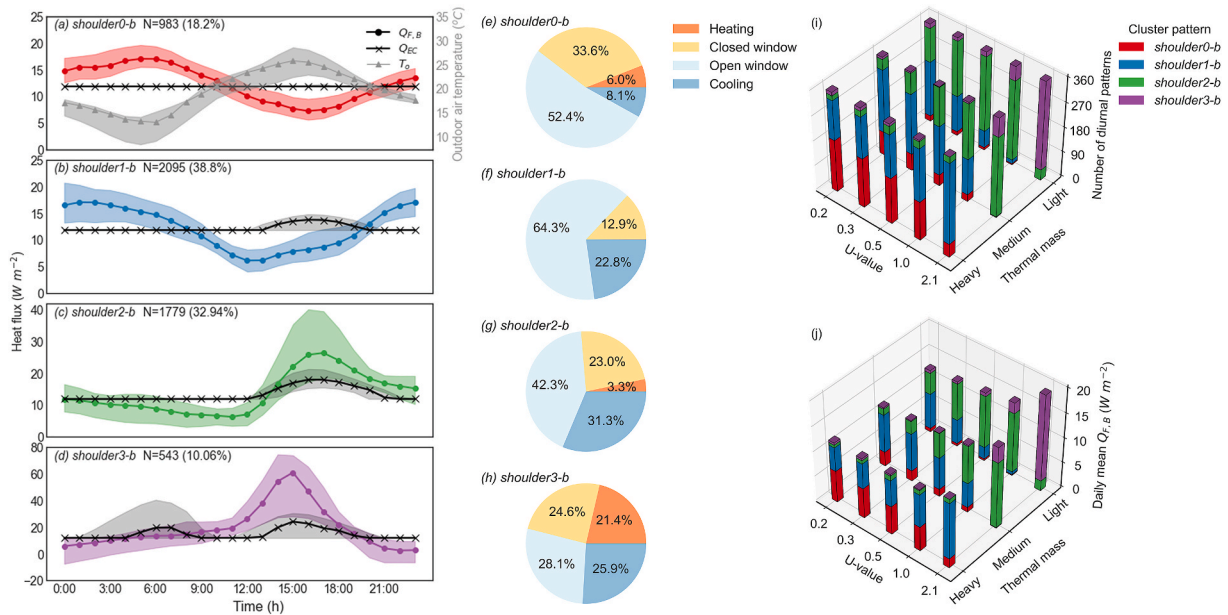


Fig. 12. As Fig. 11 but for April, May and September (AMS).

temperature. Use of both heating and cooling energy results in considerably higher daily mean $Q_{F,B}$ (Fig. 12j) than other buildings. *Shoulder2-b* has a typical summer pattern (as *summer0*) because of high cooling energy use in the afternoon when both much consumed energy and stored heat are ejected into the atmosphere. These buildings mainly are lightweight and mediumweight thermal mass with large/medium U-value, where thermal inertia effect is limited or solar heat gain through windows is relatively high.

With improving U-value or thermal mass, *shoulder1-b* become the dominant pattern, where the $Q_{F,B}$ shape is linked to heat release through natural ventilation. Peak $Q_{F,B}$ occurs at night when indoor and outdoor air temperature difference is sufficiently high and natural ventilation is used to cool the building. Pre-cooled buildings result in less cooling energy use in the afternoon. *Shoulder0-b* is dominated by natural ventilation but with a longer time with the windows closed. Most *shoulder0-b* cases have heavyweight fabrics that can minimize the use of mechanical cooling and even reduce the natural ventilation.

The effect of improving U-value varies with thermal mass level. For lightweight and mediumweight buildings, it has a moderate reduction in daily mean $Q_{F,B}$ (Fig. 12j) but shifts cooling-patterns (peak between 15:00–17:00 in Fig. 12c and d) into natural ventilation-pattern (peak between 01:00–06:00 Fig. 12a and b) with a lag of around 8–15 h. However, improving the U-value for a heavyweight building causes a negligible change in pattern and daily mean magnitude. It suggests energy-saving measures (i.e., more insulation, better glazing windows) does not reduce $Q_{F,B}$ for all buildings. Similarly, improving thermal mass also reduce magnitude and modulate the pattern for buildings with large U-value, but such effects are offset when the U-value is smaller than 0.5.

These results support the consensus that improving both U-value and thermal mass can reduce energy consumption from mechanical cooling thus impacts both diurnal pattern and magnitude of $Q_{F,B}$ in warm months. Suggesting that the appropriate designs of natural ventilation and building envelope could achieve both energy saving and modulation of the outdoor thermal environment. For example, for new construction following the high standard of insulation level in the building regulations, use of lightweight material releases most of $Q_{F,B}$ in afternoon and contributes to a smaller air temperature rise when the boundary layer is relatively deep. If buildings are difficult to insulate (e.g., solid wall), heavyweight thermal mass maybe preferred to reduce use of mechanical cooling and less heat will be released.

Overall, lightweight buildings with large U-values are likely to have

a cooling-dominated pattern, which release relatively high $Q_{F,B}$ across a day. But it will have a peak of $Q_{F,B}$ in mid-afternoon when outdoor air temperature is likely highest. Whereas, a small U-value and high thermal mass are likely to have ventilation-dominated patterns with diurnal variation offset from the outdoor air temperature. The daily $Q_{F,B}$ is small, but with a large fraction of heat released at night when the boundary layer is shallow.

3.4. Inter-season comparison

As buildings have constant properties through the year, the link between seasons is critical to understand how things will influence the fluxes at different times of the year. To do this we evaluate the impact of U-value and thermal mass on daily mean (Fig. 13) and daily peak (Fig. 14) $Q_{F,B}$ between seasons.

When cooling use is likely (summer and shoulder season warm months), improving U-value reduces both the daily mean (for 50th–95th) and peak $Q_{F,B}$ (all ranges). The reduction for lightweight buildings larger than for heavyweight buildings. The greater reduction of peak $Q_{F,B}$ for lightweight building indicate it may require higher standard insulation and glazing property to mitigate urban heating. The lightweight buildings daily peak $Q_{F,B}$ is much larger than the daily mean $Q_{F,B}$, with a daily peak to mean ratio of 1.07–7.46 in these two seasons. This highlights the importance of both sub-daily variation of $Q_{F,B}$ and that omitting the diurnal profile (e.g., one fixed value [46]) is not sufficiently accurate.

For heavyweight buildings, improving the U-value decreases minimally both the mean and peak $Q_{F,B}$ because the large heat capacity dampens the indoor temperature with less extra energy use. Enhancing thermal mass (i.e., from light-to heavyweight) may contribute to a greater reduction in peak $Q_{F,B}$ than improving insulation only. However, large heat capacity could result in a large daily mean $Q_{F,B}$ in summer when heat could be trapped in the building fabric, particularly when buildings are well insulated. The trade-off between daily mean and peak magnitude of $Q_{F,B}$ should be explored in a future study to optimize building designs for the purpose of regulating urban heating.

In heating seasons (winter and cold shoulder season months), the effect of U-value and thermal mass on daily mean and peak magnitude is relatively consistent. The U-value is the most critical parameter to modulating the magnitude. When buildings are poorly insulated, the thermal mass has a moderate influence on the magnitudes.

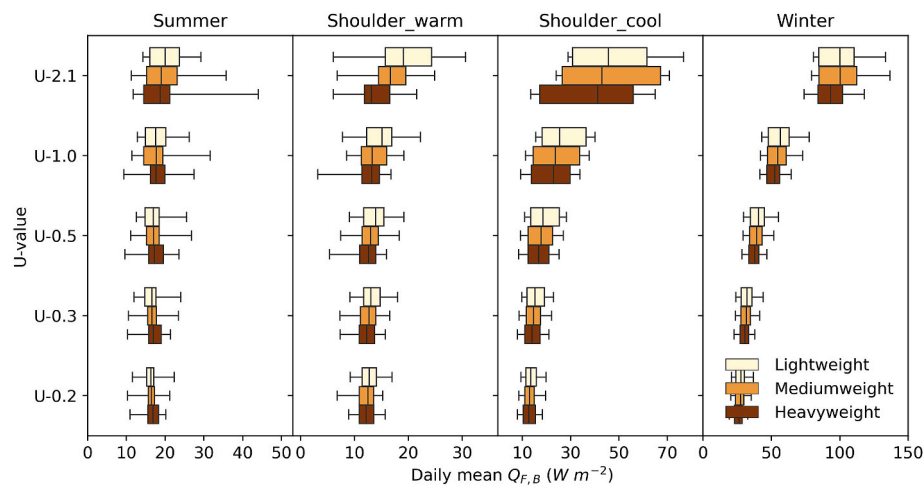


Fig. 13. Range of daily mean $Q_{F,B}$ with U-value and thermal mass by season with whiskers (5th, 95th percentile), box (25th and 75th percentile) and median (central line 50th percentile) shown. Each box contains the data varying building parameters (insulation position, windows wall ratio and orientation) and daily weather (9 days in each season). Note difference in X-scales between season.

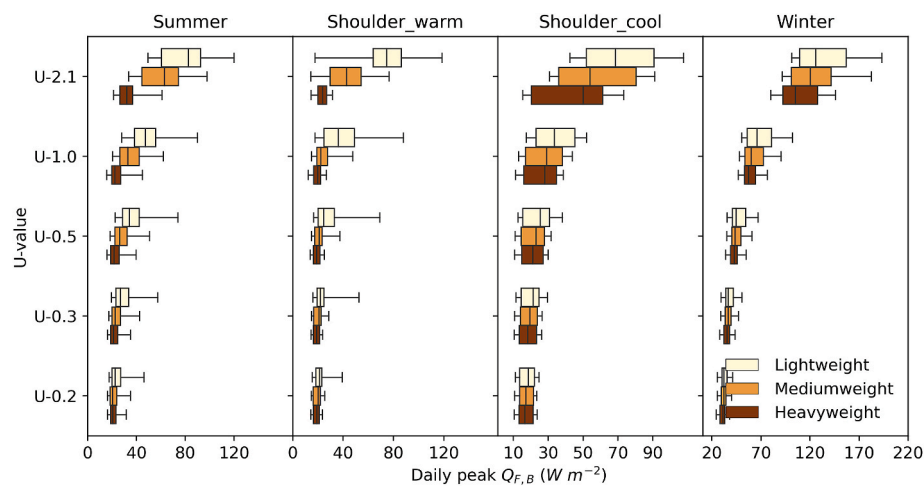


Fig. 14. As Fig. 13 but for daily peak $Q_{F,B}$.

4. Conclusions

Using K-mean clustering the representative diurnal patterns of $Q_{F,B}$ are identified, and the key building energy parameters impacting the $Q_{F,B}$ are also determined, for a city with both warm summers and cool winters (Beijing). The results address the relative importance of building parameters on $Q_{F,B}$ and provide a detailed physical understanding on how these parameters affect both diurnal patterns and mean magnitude in each season. Based on decision tree classification and distribution analysis, we find the U-value (combining thermal resistance of opaque envelope and glazing properties) is the most crucial building parameter influencing the shape of $Q_{F,B}$ diurnal patterns and this modulates the magnitude in all seasons. Thermal mass is the second most influential parameter, with its effect on $Q_{F,B}$ more pronounced in shoulder seasons with more mild outdoor weather, notably reducing daily peak $Q_{F,B}$. But such effect could be constrained by improved U-value. So both parameters emerge as important to be considered by building designers to achieve energy-saving while retaining a comfortable outdoor thermal environment. Planners should be aware of the link between building materials and anthropogenic heat fluxes, and therefore local-scale urban climates.

The key conclusions by season for this warm summer/cool winter climate are:

- In winter (DJF), improving U-values can effectively modify both diurnal pattern and reduce daily mean magnitude of $Q_{F,B}$ by up to 73%. Small U-values (e.g., U-0.2, U-0.3) can reduce heating energy demand with a limited change of storage heat flux (ΔS_{0-10}), resulting in similar pattern shape between $Q_{F,B}$ and Q_{EC} , which is offset from the diurnal outdoor air temperature variation and is barely susceptible to other building parameters. In contrast, large U-value cause large heating energy demand, with large ΔS_{0-10} , and thermal mass level becoming more important to distinguishing patterns but hardly modifying the daily $Q_{F,B}$ magnitude.
- In summer (JJA), varying U-value and thermal mass cause similar $Q_{F,B}$ diurnal cycles with different time phases (up to 3-h time lag), which also follow the diurnal variation of Q_{EC} from cooling energy use. Both parameters complement each other, the daily mean magnitude is small but the diurnal temporal phasing changes. Improving U-value reduces the $Q_{F,B}$ for lightweight buildings by reducing conduction and solar heat during the daytime. Whilst for heavyweight buildings, improved insulation traps the considerable stored heat at night, moving the peak $Q_{F,B}$ earlier.
- Shoulder seasons (the rest months) clusters are similar to winter and summer patterns, but with different dominant behaviours linked to thermal comfort because of the wide range of meteorological conditions experienced. In cool months (MON), U-value and thermal

mass play a similar role as winter, with both daily mean magnitude and pattern modulated. In warm months (AMS), low levels of insulation and thermal mass are more likely result in the $Q_{F,B}$ patterns dominated by space cooling, as in summer. Daily mean $Q_{F,B}$ is relatively large (e.g., 19.4 W m^{-2} for U-2.1 and lightweight) with most heat ejected from mid-afternoon to evening when the outdoor air temperature is high. Buildings with heavyweight fabric or small U-value are dominated by natural ventilation. With less cooling energy use, the daily mean and daily peak of $Q_{F,B}$ is smaller with up to 38% reduction in the mean and 74% in the peak (cf. U-2.1 and lightweight) and its patterns are offset (8–15h) from the peak outdoor air temperature pattern. Combined with natural ventilation, appropriate building envelope designs (e.g., large U-value with heavyweight fabric, small U-value with lightweight fabric) should be considered to achieve both building energy saving and improving outdoor thermal environment. The large sub-daily variation of $Q_{F,B}$ (e.g., daily peak to daily mean ratio is between 1.07 and 7.46 for lightweight buildings) suggests $Q_{F,B}$ should not be simplified to fixed ratios for a day. The differences in $Q_{F,B}$ diurnal pattern implies the buildings with different design parameters will have different two-way impacts on neighbourhood air temperature with potential to modify the spatial and temporal pattern of canopy layer urban heat island.

Given we demonstrate the variation of diurnal patterns of anthropogenic heat flux at the building scale, future studies should explore:

- More realistic building geometry (number of floors, roof shape etc) and internal thermal mass (internal partition and furniture).
- Our occupied (*o*) cases assume 24 h occupancy Whereas inevitably in a neighbourhood of buildings a mix will occur [47]. A mix of schedules should be used as they would modify diurnal patterns of Q_{EC} and therefore $Q_{F,B}$.
- Our unoccupied (*uo*) baseline is ideally sealed but other cases (other scenarios in [1]) should be used.
- Different climates and/or different socio-economic cultures will modify thermal comfort norms and/or the influence of building parameters, particularly for natural ventilation and nocturnal temperature in summer and shoulder season.
- $Q_{F,B}$ impacts buildings, its feedback on neighbourhood scale and therefore the building climate. Better understanding the feedback between the two will help to bridge building design, local scale and urban climate.

CRediT authorship contribution statement

Yiqing Liu: Visualization, Methodology, Formal analysis, Data curation, Conceptualization, Writing – original draft, Writing – review & editing. **Zhiwen Luo:** Supervision, Project administration, Methodology, Funding acquisition, Formal analysis, Conceptualization, Writing – review & editing. **Sue Grimmond:** Supervision, Project administration, Methodology, Funding acquisition, Conceptualization, Writing – review & editing.

Declaration of competing interest

The authors declare no financial interests.

Data availability

Information on the data underpinning the results presented here can be found at <https://zenodo.org/record/7665298> (Liu et al., 2023).

Acknowledgement

This work has been funded as part of NERC-COSMA project (NE/

S005889/1), ERC urbisphere (855005) and Newton Fund/Met Office CSSP-China (SG, ZL, YL).

Appendix A. Supplementary data

Supplementary data to this article can be found online at <https://doi.org/10.1016/j.buildenv.2023.110134>.

References

- [1] Y. Liu, Z. Luo, S. Grimmond, Revising the definition of anthropogenic heat flux from buildings: role of human activities and building storage heat flux, *Atmos. Chem. Phys.* 22 (2022) 4721–4735, <https://doi.org/10.5194/acp-2021-914>.
- [2] United Nations, Department of economic and social affairs, Population Division: *World Urbanization Prospects: the 2018 Revision ST/ESA/SER.A/420*, New York, 2019.
- [3] WMO, Guidance to measuring, modelling and monitoring the canopy layer urban heat island (CL-UHI), in: K.H. Schlünzen, S. Grimmond, A. Baklanov (Eds.), *World Meteorological Organization (WMO)*, 2023. WMO-No. 1292 Available at, https://library.wmo.int/index.php?lvl=notice_display&id=22236#.ZAC203bP1PY. (Accessed 2 March 2023).
- [4] H. Fan, D.J. Sailor, Modeling the impacts of anthropogenic heating on the urban climate of Philadelphia: a comparison of implementations in two PBL schemes, *Atmos. Environ.* 39 (1) (2005) 73–84, <https://doi.org/10.1016/j.atmosenv.2004.09.031>.
- [5] M. Santamouris, N. Papanikolaou, I. Livada, I. Koronakis, C. Georgakis, A. Argiriou, D.N. Assimakopoulos, On the impact of urban climate on the energy consumption of building, *Sol. Energy* 70 (3) (2001) 201–216, [https://doi.org/10.1016/S0038-092X\(00\)00095-5](https://doi.org/10.1016/S0038-092X(00)00095-5).
- [6] A. Milojevic, P. Wilkinson, B. Armstrong, M. Davis, A. Mavrogianni, S. Bohnenstengel, S. Belcher, Impact of London's urban heat island on heat-related mortality, *Epidemiology* 22 (1) (2011), <https://doi.org/10.1097/01.ede.0000392239.91165.65>.
- [7] C. Heaviside, S. Vardoulakis, X.M. Cai, Attribution of mortality to the urban heat island during heatwaves in the West Midlands, UK, *Environ. Heal. A Glob. Access Sci. Source* 15 (Suppl 1) (2016), <https://doi.org/10.1186/s12940-016-0100-9>.
- [8] T.R. Oke, G. Mills, A. Christen, J.A. Voogt, *Urban Climates, Anthropogenic heat flux*, Cambridge University Press, 2017, pp. 463–479.
- [9] Y. Ohashi, Y. Genchi, H. Kondo, Y. Kikigawa, H. Yoshikado, Y. Hirano, Influence of air-conditioning waste heat on air temperature in Tokyo during summer: numerical experiments using an urban canopy model coupled with a building energy model, *J. Appl. Meteorol. Climatol.* 46 (1) (2007) 66–81, <https://doi.org/10.1175/JAM2441.1>.
- [10] Y. Chen, W.M. Jiang, N. Zhang, X.F. He, R.W. Zhou, Numerical simulation of the anthropogenic heat effect on urban boundary layer structure, *Theor. Appl. Climatol.* 97 (2009) 123–134, <https://doi.org/10.1007/s00704-008-0054-0>.
- [11] F. Salamanca, M. Georgescu, A. Mahalov, M. Moustauoui, M. Wang, Anthropogenic heating of the urban environment due to air conditioning, *J. Geophys. Res. Atmos. Res.* 119 (2014) 5945–5965, <https://doi.org/10.1038/175238c0>.
- [12] P. Vahmani, X. Luo, A. Jones, T. Hong, Anthropogenic heating of the urban environment: an investigation of feedback dynamics between urban micro-climate and decomposed anthropogenic heating from buildings, *Build. Environ.* 213 (2022), 108841, <https://doi.org/10.1016/j.buildenv.2022.108841>.
- [13] D. Narumi, A. Kondo, Y. Shimoda, Effects of anthropogenic heat release upon the urban climate in a Japanese megacity, *Environ. Res.* 109 (4) (2009) 421–431, <https://doi.org/10.1016/j.envres.2009.02.013>.
- [14] S.I. Bohnenstengel, I. Hamilton, M. Davies, S.E. Belcher, Impact of anthropogenic heat emissions on London's temperatures, *Q. J. R. Meteorol. Soc.* 140 (679) (2014) 687–698, <https://doi.org/10.1002/qj.2144>.
- [15] L. Allen, F. Lindberg, C.S.B. Grimmond, Global to city scale urban anthropogenic heat flux: model and variability, *Int. J. Climatol.* 31 (13) (2011) 1990–2005, <https://doi.org/10.1002/joc.2210>.
- [16] T. Hong, M. Ferrando, X. Luo, F. Causone, Modeling and analysis of heat emissions from buildings to ambient air, *Appl. Energy* 277 (2020), 115566, <https://doi.org/10.1016/j.apenergy.2020.115566>.
- [17] I. Korolija, L. Marjanovic-Halburd, Y. Zhang, V.I. Hanby, UK office buildings archetypal model as methodological approach in development of regression models for predicting building energy consumption from heating and cooling demands, *Energy Build.* 60 (2013) 152–162, <https://doi.org/10.1016/j.enbuild.2012.12.032>.
- [18] H. Samuelson, S. Claussnitzer, A. Goyal, Y. Chen, A. Romo-Castillo, Parametric energy simulation in early design: high-rise residential buildings in urban contexts, *Build. Environ.* 101 (2016) 19–31, <https://doi.org/10.1016/j.buildenv.2016.02.018>.
- [19] R. Yao, V. Costanzo, X. Li, Q. Zhang, B. Li, The effect of passive measures on thermal comfort and energy conservation. A case study of the hot summer and cold winter climate in the Yangtze River region, *J. Build. Eng.* 15 (2018) 298–310, <https://doi.org/10.1016/j.jobte.2017.11.012>.
- [20] H. Yoshino, Y. Yoshino, Q. Zhang, A. Mochida, N. Li, Z. Li, H. Miyasaka, Indoor thermal environment and energy saving for urban residential buildings in China, *Energy Build.* 38 (11) (2006) 1308–1319, <https://doi.org/10.1016/j.enbuild.2006.04.006>.

- [21] E. Oikonomou, M. Davies, A. Mavrogianni, P. Biddulph, P. Wilkinson, M. Kolokotroni, Modelling the relative importance of the urban heat island and the thermal quality of dwellings for overheating in London, *Build. Environ.* 57 (2012) 223–238, <https://doi.org/10.1016/j.buildenv.2012.04.002>.
- [22] Y. Ji, I. Korolija, Y. Zhang, Thermal responses of single zone offices on existing near-extreme summer weather data, *Build. Simulat.* 11 (2018) 15–35, <https://doi.org/10.1007/s12273-017-0367-y>.
- [23] D. Fosas, D.A. Coley, S. Natarajan, M. Herrera, M. Fosas de Pando, A. Ramallo-Gonzalez, Mitigation versus adaptation: does insulating dwellings increase overheating risk? *Build. Environ.* 143 (2018) 740–759, <https://doi.org/10.1016/j.buildenv.2018.07.033>.
- [24] P.T. Tsilingiris, Parametric space distribution effects of wall heat capacity and thermal resistance on the dynamic thermal behavior of walls and structures, *Energy Build.* 38 (10) (2006) 1200–1211, <https://doi.org/10.1016/j.enbuild.2006.02.007>.
- [25] F. Leccese, G. Salvadori, F. Asdrubali, P. Gori, Passive thermal behaviour of buildings: performance of external multi-layered walls and influence of internal walls, *Appl. Energy* 225 (2018) 1078–1089, <https://doi.org/10.1016/j.apenergy.2018.05.090>.
- [26] MOHURD, Design Standard for Energy Efficiency of Residential Building in Severe Cold and Cold Zones, JGJ 26-1995, Ministry of Housing and Urban-Rural, 1995 (in Chinese).
- [27] MOHURD, Design Standard for Energy Efficiency of Residential Building in Severe Cold and Cold Zones, JGJ 26-2010, Ministry of Housing and Urban-Rural, 2010 (in Chinese).
- [28] MOHURD, Design Standard for Energy Efficiency of Residential Building in Severe Cold and Cold Zones, JGJ 26-2018, Ministry of Housing and Urban-Rural, 2018 (in Chinese).
- [29] China Meteorological Bureau, Climate Information Center, Climate Data Office and Tsinghua University, Department of Building Science and Technology: China Standard Weather Data for Analyzing Building Thermal Conditions, China Building Industry Publishing House, Beijing, 2005. ISBN 7-112-07273-3 (13228).
- [30] jEPlus, jEPlus – Java shell for E+ parametrics, 2012. <http://sourceforge.net/projects/jeplus/>. (Accessed 1 October 2022).
- [31] DOE, EnergyPlus™ version 9.4.0, 2020. <https://energyplus.net/>.
- [32] Y. Zhao, C. Zhang, Y. Zhang, Z. Wang, J. Li, A review of data mining technologies in building energy systems: load prediction, pattern identification, fault detection and diagnosis, *Energy Built Environ.* 1 (2) (2020) 149–164, <https://doi.org/10.1016/j.enbenv.2019.11.003>.
- [33] G. Chicco, Overview and performance assessment of the clustering methods for electrical load pattern grouping, *Energy* 42 (1) (2012) 68–80, <https://doi.org/10.1016/j.energy.2011.12.031>.
- [34] J.Y. Park, X. Yang, C. Miller, P. Arjunan, Z. Nagy, Apples or oranges? Identification of fundamental load shape profiles for benchmarking buildings using a large and diverse dataset, *Appl. Energy* 236 (2019) 1280–1295, <https://doi.org/10.1016/j.apenergy.2018.12.025>.
- [35] X. Luo, T. Hong, Y. Chen, M.A. Piette, Electric load shape benchmarking for small- and medium-sized commercial buildings, *Appl. Energy* 204 (2017) 715–725, <https://doi.org/10.1016/j.apenergy.2017.07.108>.
- [36] P. Gianniou, X. Liu, A. Heller, P.S. Nielsen, C. Rode, Clustering-based analysis for residential district heating data, *Energy Convers. Manag.* 165 (2018) 840–850, <https://doi.org/10.1016/j.enconman.2018.03.015>.
- [37] J. Sala, R. Li, M.H. Christensen, Clustering and classification of energy meter data: a comparison analysis of data from individual homes and the aggregated data from multiple homes, *Build. Simulat.* 14 (2021) 103–117, <https://doi.org/10.1007/s12273-019-0587-4>.
- [38] S. Yilmaz, J. Chambers, M.K. Patel, Comparison of clustering approaches for domestic electricity load profile characterisation - implications for demand side management, *Energy* 180 (2019) 665–677, <https://doi.org/10.1016/j.energy.2019.05.124>.
- [39] P.J. Rousseeuw, Silhouettes: a graphical aid to the interpretation and validation of cluster analysis, *J. Comput. Appl. Math.* 20 (1987) 53–65, [https://doi.org/10.1016/0377-0427\(87\)90125-7](https://doi.org/10.1016/0377-0427(87)90125-7).
- [40] U. Maulik, S. Bandyopadhyay, Performance evaluation of some clustering algorithms and validity indices, *IEEE Trans. Pattern Anal. Mach. Intell.* 24 (12) (2002) 1650–1654, <https://doi.org/10.1109/TPAMI.2002.1114856>.
- [41] M. Schonlau, The clustergram: a graph for visualizing hierarchical and nonhierarchical cluster analyses, *STATISTICS* 2 (4) (2002) 391–402, <https://doi.org/10.1177/1536867X0200200405>.
- [42] P. Anuja, A. Rahul, G.A. Ratheeb, S. Srivastavab, Comparative analysis of decision tree classification algorithms, *Int. J. Curr. Eng. Technol.* 3 (2) (2013) 334–337.
- [43] L.E. Raileanu, K. Stoffel, Theoretical comparison between the gini index and information gain criteria, *Ann. Math. Artif. Intell.* 41 (1) (2004) 77–93, <https://doi.org/10.1023/B:AMAI.0000018580.96245.c6>.
- [44] S. Verbeke, A. Audenaert, Thermal inertia in buildings: a review of impacts across climate and building use, *Renew. Sustain. Energy Rev.* 82 (2018) 2300–2318, <https://doi.org/10.1016/j.rser.2017.08.083>.
- [45] S.M. Porritt, P.C. Cropper, L. Shao, C.I. Goodier, Ranking of interventions to reduce dwelling overheating during heat waves, *Energy Build.* 55 (2012) 16–27, <https://doi.org/10.1016/j.enbuild.2012.01.043>.
- [46] C.S.B. Grimmond, M. Blackett, M.J. Best, J. Barlow, J.J. Baik, S.E. Belcher, S. I. Bohnenstengel, I. Calmet, F. Chen, A. Dandou, K. Fortuniak, M.L. Gouvea, R. Hamdi, M. Hendry, T. Kawai, Y. Kawamoto, H. Kondo, E.S. Krayenhoff, S.H. Lee, T. Loridan, A. Martilli, V. Masson, S. Miao, K. Oleson, G. Pigeon, A. Porson, Y. H. Ryu, F. Salamanca, L. Shashua-Bar, G.J. Steeneveld, M. Tombrou, J. Voogt, D. Young, N. Zhang, The international urban energy balance models comparison project: first results from phase 1, *J. Appl. Meteorol. Climatol.* 49 (6) (2010) 1268–1292, <https://doi.org/10.1175/2010JAMC2354.1>.
- [47] I. Capel-Timms, S.T. Smith, T. Sun, S. Grimmond, Dynamic Anthropogenic activities impacting Heat emissions (DASH v1.0): development and evaluation, *Geosci. Model Dev. (GMD)* 13 (10) (2020) 4891–4924, <https://doi.org/10.5194/gmd-13-4891-2020>.